SHM
Structural Health Monitoring

Piezoelectric Wafer Embedded Active Sensors for Aging Aircraft Structural Health Monitoring

Victor Giurgiutiu,* Andrei Zagrai and Jing Jing Bao

Department of Mechanical Engineering, University of South Carolina, 300 South Main St., Columbia, SC, 29212, USA

Piezoelectric wafer active sensors may be applied on aging aircraft structures to monitor the onset and progress of structural damage such as fatigue cracks and corrosion. The state of the art in piezoelectric-wafer active sensors structural health monitoring and damage detection is reviewed. Methods based on (a) elastic wave propagation and (b) the Electro–Mechanical (E/M) impedance technique are cited and briefly discussed. For health monitoring of aging aircraft structures, two main detection strategies are considered: the E/M impedance method for near field damage detection, and wave propagation methods for far-field damage detection. These methods are developed and verified on simple-geometry specimens and on realistic aging aircraft panels with seeded cracks and corrosion. The experimental methods, signal processing, and damage detection algorithms are tuned to the specific method used for structural interrogation. In the E/M impedance method approach, the high-frequency spectrum, representative of the structural resonances, is recorded. Then, overall-statistics damage metrics can be used to compare the impedance signatures and correlate the change in these signatures with the damage progression and intensity. In our experiments, the $(1 - R^2)^3$ damage metric was found to best fit the results in the 300–450 kHz band. In the wave propagation approach, the pulse-echo and acousto-ultrasonic methods can be utilized to identify the additional reflections generated from crack damage and the changes in transmission phase and velocity associated with corrosion damage. The paper ends with a conceptual design of a structural health monitoring system and suggestions for aging aircraft installation utilizing active-sensor arrays, data concentrators, wireless transmission, and a health monitoring and processing unit.

Keywords piezoelectric sensors · active sensors · aging aircraft · damage detection · structural health monitoring · failure prevention · ultrasonics · pulse-echo · emitter-receptor · acousto-ultrasonic · signal analysis · electromechanical (E/M) impedance · pointwise impedance · pulse-echo · wireless transmission · data concentrators

1 Introduction

Health monitoring of aging structures is a major concern of the engineering community. This need is even more intense in the case of aging aerospace structures, which have been operating well beyond their initial design life. Multi-site fatigue damage, hidden cracks in hard-to-reach locations, and corrosion are among the major flaws encountered in today's extensive fleet of aging aircraft and space vehicles. The durability and health monitoring of such structures form the subject of

*Author to whom correspondence should be addressed.
E-mail: victorg@sc.edu

Vol 1(1): 0041–61
[1475-9217 (200207) 1:1;41–61; 026548]

extensive research in many universities, government labs, and industry. This area is worthy of new and innovative approaches. The nation's safety and reliability record is excellent, but the fatigue of its aging aerospace fleet is raising major concerns. An assessment is needed of how the aircraft airworthiness is effected by aging, and by the dangerous combination between fatigue and corrosion. Prevention of such unexpected occurrences could be improved through the installation of on-board health monitoring systems that could assess the structural integrity and detect incipient damage before catastrophic failure occurs. To gain widespread acceptance, such a system has to be cost-effective, reliable, compact, and lightweight.

The use of condition-based maintenance coupled with continuous on-line structural integrity monitoring could significantly reduce the cost of the inspection programs. Retirement-for-cause instead of retirement-as-planned could reduce the cost while maintaining a safe operation life for many aging aircraft structures. The replacement of our present-day manual inspection with automatic health monitoring would substantially reduce the associated lifecycle costs. Hence, there is a need for reliable structural health monitoring systems that can automatically process data, assess structural condition, and signal the need for corrective action. Motivated by these needs, considerable research effort is being currently directed towards (a) development of new and better nondestructive inspection (NDI) techniques; (b) subjecting the aging fleet to life-enhancement and life-extension treatments; and (c) improving the inspection and maintenance procedures to better capture unexpected occurrences (Bartkowicz, et al., 1996). At the same time, efforts are focused on: (a) the development of specialized health monitoring sensors; and (b) the construction of automated health-monitoring systems.

Among the available options for on-board structural health monitoring systems, the piezo-electric-wafer active sensors have the advantage of being slim and unobtrusive, readily integrated into structures, and self-excited. Self-excitation ensures that no cumbersome electrical excitation devices are required and that small-size electronics can be developed to accommodate the tight space and weight requirements of most aircraft structures. Health monitoring sensors based on active-material principles constitute an enabling technology of keen interest (Boller et al., 1999). Conventional passive sensors can only tell what happened to the structure, i.e., load and strain history. In contrast, active sensors are able to interrogate the structure (e.g., through elastic waves) and find out "how it feels", i.e. the state of its health. Active sensors can act as both transmitters and receptors. As transmitters, they generate elastic waves in the surrounding material. As receptors, they receive elastic waves and transform them into electric signals. In active-sensor arrays, each element would take, in turn, the role of transmitter and receptor, and thus scan large structural areas using ultrasonic waves. Alternatively, local-area impedance interrogation can be achieved by individual active sensors, which are simultaneously transmitters and receptors and generate standing waves. Piezoelectric-wafer active sensors have the potential to bring about a revolution in structural health monitoring, damage detection, and non-destructive evaluation just as significant as ultrasonic inspection did half a century ago.

2 Piezoelectric-Wafer Active Sensors

Piezoelectric-wafer active sensors (PWAS) are small, non-intrusive, inexpensive, wide-band elastic wave generators/receptors, which can be intimately affixed to a structure and can actively interrogate it (Giurgiutiu and Zagrai, 2000a; Giurgiutiu et al., 2002). PWAS are commonly manufactured from thin wafers of the piezoceramic $Pb(Zr–Ti)O_3$ (a.k.a. PZT). Unlike conventional ultrasonic transducer, PWAS are non-resonant devices with wide frequency-band capabilities. They can be wired into sensor arrays that can be connected to data concentrators and wireless communicators. PWAS have captured the interest of academic and industrial communities due to their low cost and small non-intrusive nature (Bartkowicz et al., 1996; Boller et al., 1999).

The general constitutive equations of linear piezo-electric material behavior, as given by

ANSI/IEEE Standard 176-1987, describe a tensorial relation between mechanical and electrical variables (mechanical strain, S_{ij}, mechanical stress, T_{kl}, electrical field, E_k, and electrical displacement D_j) in the form:

$$S_{ij} = s^E_{ijkl} T_{kl} + d_{kij} E_k$$
$$D_j = d_{jkl} T_{kl} + \varepsilon^T_{jk} E_k, \quad (1)$$

where s^E_{ijkl} is the mechanical compliance of the material measured at zero electric field ($E=0$), ε^T_{jk} is the dielectric permittivity measured at zero mechanical stress ($T=0$), and d_{kij} is the piezoelectric coupling between the electrical and mechanical variables. The *direct piezo-electric effect* is reflected in the second equation, while the first equation refers to the *converse piezo-electric effect*. In PWAS configuration, the mechanical stresses and strains are applied in the 1- and 2-directions, i.e. in the plane of the surface, while the electric field acts in the 3-direction, i.e., normal to the surface. Hence, the relevant electro-mechanical couplings for this analysis are the 3-1 and 3-2 effects. The application of an electric field, E_3, induces surface strains, S_{11} and S_{22}, and vice-versa. The PWAS is intimately bonded to the structure, such that the strain/displacement compatibility and stress/force equilibrium principles apply. As the piezoelectric material is electrically activated, strain is induced in the PWAS, and interaction forces and moments appear at the interface between the sensor and the structure. Conversely, when an elastic wave travels through the structure, the PWAS gets activated through the strain/displacement compatibility condition. In accordance with Equation (1), the strain induced in the PWAS generates an electric field that is captured as voltage at the PWAS terminals.

3 State of the Art in Conventional and Active-sensor Damage Detection and Structural Health Monitoring

Among the various NDI techniques, those based on elastic waves, such as ultrasonics, acousto-ultrasonics, and mechanical impedance, are prominent. Ultrasonics relies on elastic wave propagation and their reflection/scattering from the field inhomogeneities due to local damage and flaws. Ultrasonic testing involves one or more of the following measurements: time of wave transit (or delay), path length, frequency, phase angle, amplitude, impedance, and angle of wave deflection (reflection and refraction). Conventional ultrasonic methods include the pulse-echo, the pulse-transmission (or shadow), and the pulse-resonance techniques (Krautkramer and Krautkramer, 1990; Blitz and Simpson, 1996). Advanced ultrasonic techniques rely on the generation, propagation, and detection of Rayleigh, Lamb, and Love waves (Viktorov, 1967). Such guided waves can travel at large distances with little amplitude loss. Further advancement in this direction was achieved through acousto-ultrasonics (Duke, 1988).

The *mechanical impedance method* is a damage detection technique complementary to the wave propagation techniques. The mechanical impedance method was pioneered by Lange (1978) and Cawley (1984). Ultrasonic equipment manufacturers (e.g., Staveley NDT Technologies, 1998) offer, as options, mechanical impedance analysis (MIA) probes that consist of specialized ultrasonics transducers that simultaneously measure the applied normal force and the induced velocity. For disbond detection, the high-frequency vibrations of bonded plates are excited, and disbond presence is deduced from the change in the apparent mechanical impedance.

The drawbacks of the ultrasonic techniques are the bulkiness of the transducers and the need for a normal (perpendicular) interface between the transducer and the test structure. In contrast, the piezoelectric-wafer active-sensors are small, thin, unobtrusive, and non-invasive. They can be placed in small spaces and inside built-up aerospace structures. Through their adhesive coupling with the structure, the PWAS can directly produce guided waves traveling parallel to the surface. In addition, because of their low cost and size, the PWAS can be installed in sensor arrays to cover large surfaces, which would be prohibitively expensive and obtrusive if conventional ultrasonic transducers were used.

The use of PWAS for damage detection using wave propagation was pioneered by Chang (1995). Moetakef et al. (1996) studied theoretically and experimentally the elastic-wave generation by PWAS. Chang (1988, 2001), Wang and Chang (2000), and Ihn and Chang (2002) studied the use of PWAS for generation and reception of elastic waves in composite materials. Blanas et al. (1998) developed embedded flexible PWAS for acoustic-emission detection in composite materials. Jiang, et al. (1999), Deng et al. (1999), and Lemistre et al. (1999) detected damage with PWAS-generated waves and wavelet transforms. Dupont et al. (2000) and Osmont et al. (2000a, b) used PWAS to detect damage impacts. Giurgiutiu et al. (2001a) studied theoretically and experimentally PWAS for pulse-echo damage detection.

Electromechanical impedance method was pioneered by Liang et al. (1994) and Sun et al. (1994, 1995). Subsequently, several authors used the E/M impedance method for structural health monitoring, by comparing the impedance frequency spectra of various pristine and damaged structures (Chaudhry et al., 1994, 1995; Ayres et al., 1996; Giurgiutiu et al., 1998, 2002; Park et al., 2000a, 2001; Giurgiutiu and Zagrai, 2000b). The method has been shown to be especially effective at ultrasonic frequencies, which properly capture the changes in local dynamics due to incipient structural damage. (Such changes are too small to affect the global dynamics and hence cannot be readily detected by conventional low-frequency vibration methods). The name *Electro–Mechanical (E/M) Impedance Method* was first used by Giurgiutiu and Rogers (1997). Novel ways to interpret the E/M impedance spectra and identify structural damage have been explored by Quin et al. (1999), Lopez et al. (2000); Park et al. (2000b), Tseng et al. (2000), Monaco et al. (2001). The essence of the E/M impedance method is illustrated in Figure 1. The apparent E/M impedance of the PWAS as coupled to the host structure is:

$$Z(\omega) = \left[i\omega C \left(1 - \kappa_{31}^2 \frac{Z_{\text{str}}(\omega)}{Z_{\text{PWAS}}(\omega) + Z_{\text{str}}(\omega)} \right) \right]^{-1} \tag{2}$$

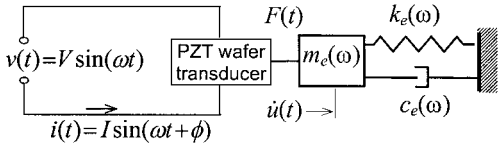

Figure 1 Electro-mechanical coupling between the PZT active sensor and the structure.

where $Z(\omega)$ is the equivalent electro-mechanical admittance as seen at the PZT active sensor terminals, C is the zero-load capacitance of the PZT active sensor, κ_{31} is the electr-mechanical cross coupling coefficient of the PWAS ($\kappa_{31} = d_{13}/\sqrt{\bar{s}_{11}\bar{\varepsilon}_{33}}$), Z_{str} is the impedance of the structure, and Z_{PWAS} is the impedance of the piezoelectric-wafer active sensor.

In this paper, we present a set of experiments in which both the E/M impedance technique and the wave propagation methods are used for damage detection, thus showing that the two approaches are complementary and can be used with the same PWAS installation.

4 Experimental Setup

4.1 Test Specimens and Apparatus

The test specimens were constructed for two purposes: (a) to develop and calibrate the damage-detection methodology using simple-geometry specimens; and (b) to demonstrate damage detection on realistic specimens representative of aging aircraft structures. The simple-geometry specimens included thin-gauge strips and plates. The realistic aging aircraft specimens were fabricated at Sandia National Labs with simulated aging-like induced damage (cracks and corrosion). These specimens had a built-up construction typical of conventional aircraft structures (Figure 2). Each specimen features a lap splice, tear straps, and hat-shaped stringer/stiffeners, and is made of 1-mm (0.040″) 2024-T3 Al-clad sheet assembled with 4.2-mm (0.166″) diameter countersunk rivets. Cracks were simulated using the Electric Discharge Machining (EDM) process and consisted of hairline through-the-thickness slits of various lengths (5–25 mm).

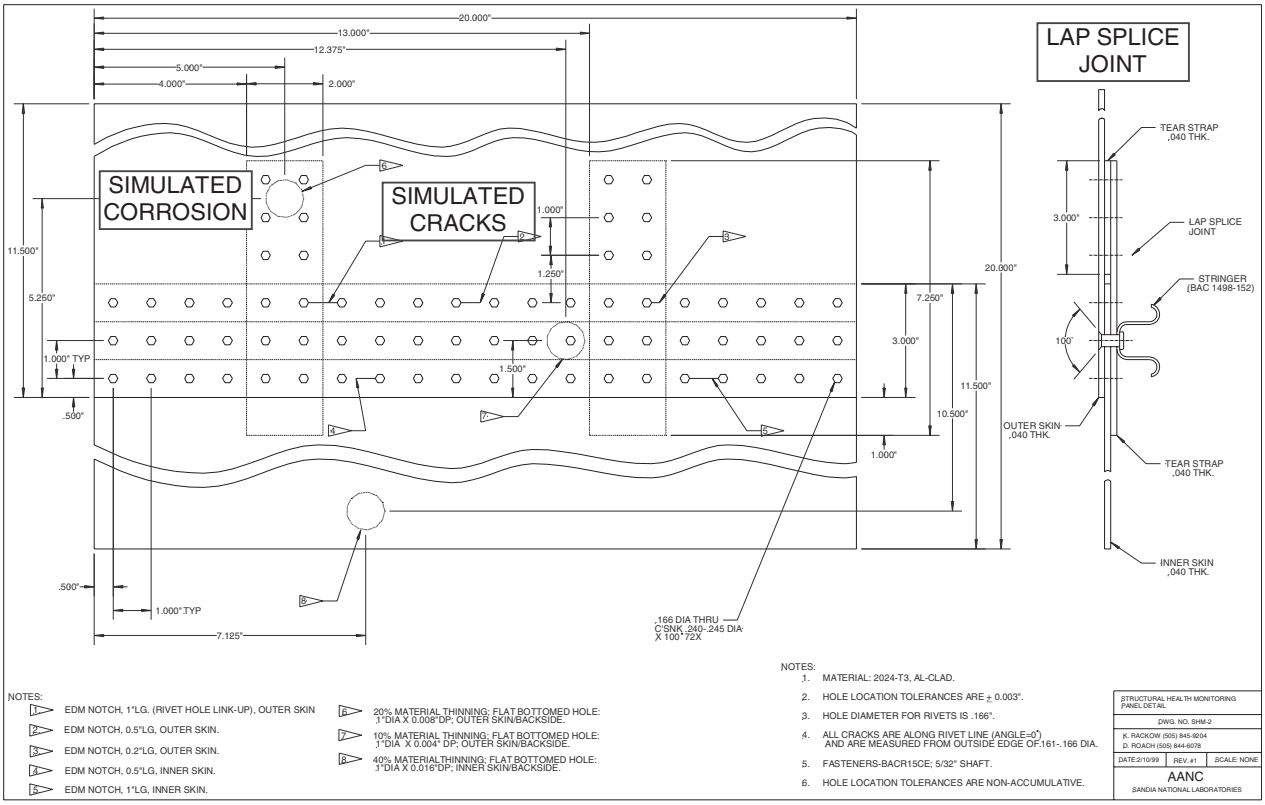

Figure 2 Blue print of the experimental panels developed at Sandia National Laboratories as specimens for testing active-sensor structural health monitoring, damage detection, and failure prevention methodologies. The specimen has a built-up construction typical of conventional aircraft structures. It contains simulated cracks (EDM hairline slits) and simulated corrosion damage (chem.-milled areas).

Corrosion damage was simulated using the chemical milling (Chem.-Milled) process by removing between 10% and 40% of the material thickness from several 25.4 mm diameter areas, as detailed in Figure 2. The specimens were instrumented with circular and rectangular PWAS (0.2 mm thick, 7-mm diameter or 7-mm square). The PWAS were bonded to the specimens with Micro Measurements, Inc. M-Bond 200 fast action adhesive, and instrumented with thin-gage leads. The common ground negative pole was provided by the test specimen. For E/M impedance experiments, the experimental apparatus consisted of a HP 4194A impedance analyzer. For wave propagation experiments, an HP 33120 wave-generator, Tektronix TDS 210 digital oscilloscope, Trek 50/750 HV amplifier, and data acquisition laptop PC with PCMCIA GPIB card were used.

4.2 Active Sensor Calibration and Self-Diagnostics

The state of the piezoelectric-wafer active sensors (PWAS) affixed to, or embedded into the structure plays a major role in the successful operation of the health monitoring and damage detection system. We studied the calibration of PWAS before and after installation, and found that consistent and repetitive results can be obtained when careful sensor screening and consistent adherence to sensor installation procedures are enforced (Figure 3a). After installation, sensor integrity and consistency over long periods of operation are of utmost importance for successful structural health monitoring. The general expectation is that, once the active sensors have been placed onto or into the structure, they will behave consistently throughout the duration

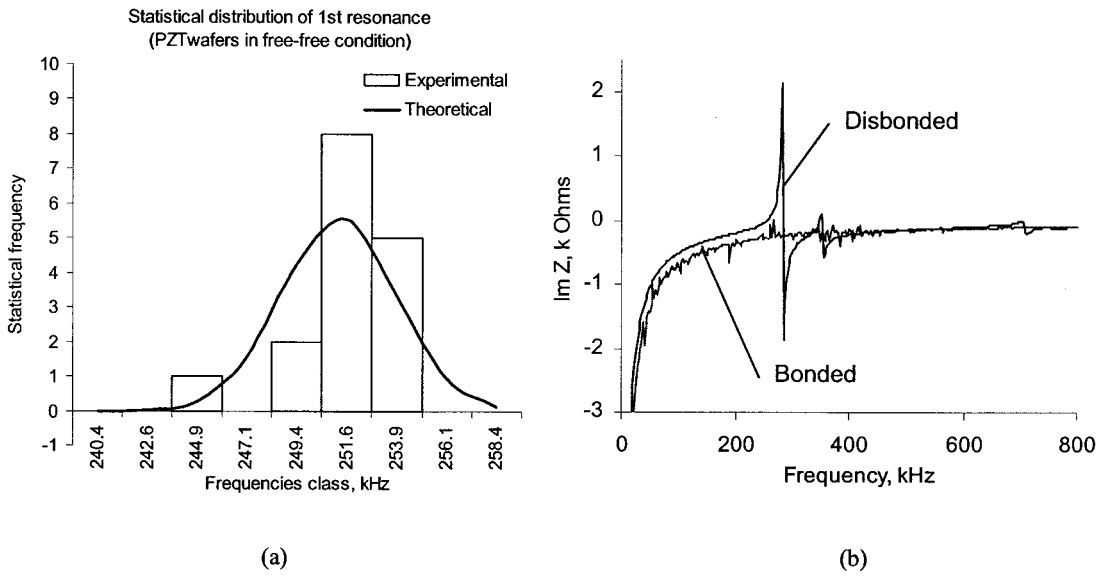

Figure 3 PWAS calibration and self-diagnostic: (a) statistics of a PWAS batch showed consistency of first-resonance from Re Z measurements; (b) PWAS self diagnostic with Im Z: when sensor is disbonded, a new free-vibration resonance appears at 267 kHz.

of the health monitoring exercise, which may encompass various service conditions and several loading cases, over several years and even decades. The sensor–structure adhesion may be affected by both humidity and temperature. Cycling of humidity and temperature may affect the sensor–structure adhesive interface and promote disbonding. Therefore, in-situ self-diagnostics of sensor integrity and sensor-to-structure adhesion are mandatory. We identified a sensor self-test procedure (Giurgiutiu et al., 2002) that can reliably determine if the sensor is still perfectly attached to the structure, or not. Figure 3b compares the Im Z spectrum of a well-bonded sensor with that of a disbonded (free) sensor. The well-bonded sensor presents a smooth Im Z curve, modulated by small structural-resonance features. The disbonded sensor shows a very strong sensor resonance, and no structural resonances. The appearance of sensor resonance, and the disappearance of structural resonances constitute unambiguous features that tell when the sensor has become disbonded. This feature can be used for automated sensor self-diagnostics. Similar results were also obtained for partially bonded sensors. In this case, a mixture of sensor vibration and structure vibration was recorded. These experiments have shown that positive identification of defective sensor installation is possible, and that progressive degradation of sensor adherence to the structure can be experimentally traced.

5 E/M Impedance Damage Detection Experiments

5.1 E/M Impedance Experiments on Simple-Geometry Specimens

A series of experiments on simple geometry specimens (thin-gage aluminum circular plates) was conducted for assessing and calibrating the E/M impedance method. Twenty-five plate specimens (100-mm diameter, 1.6-mm thick) were constructed from aircraft-grade 2024-T3 aluminum-alloy sheet. Each plate was instrumented with one 7-mm diameter PWAS placed at its center (Figure 4a). A 10-mm circumferential EDM slit was used to simulate an in-service crack. The crack was placed at increasing distance from the sensor (Figure 4b and Table 1). Thus, five groups of five identical plates were obtained. E/M impedance data was taken using an HP 4194A

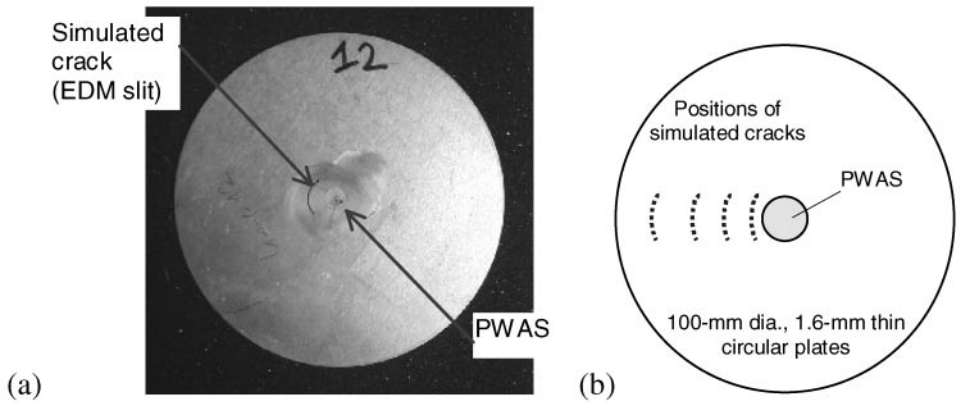

Figure 4 Systematic study of E/M impedance technique on circular plates: (a) Photograph of actual specimen showing a 7-mm piezoelectric-wafer active sensor (PWAS) and a simulated crack (EDM slit); (b) progression of specimen geometries with simulated cracks (slits) at decreasing radial distances.

Table 1 Systematic study of the E/M impedance technique on circular plates: identification of the five statistical groups of specimens with seeded cracks at various locations.

Group ID	*0*	*1*	*2*	*3*	*4*
r (mm)	50	40	25	10	3
No. of specimens	5	5	5	5	5

Impedance Analyzer. During the experiments, the specimens were supported on packing foam to simulate free–free conditions.

The experiments were conducted over three frequency bands: 10–40 kHz, 10–150 kHz and 300–450 kHz. The data was processed by considering the real part of the E/M impedance spectrum, and determining a damage metric to quantify the difference between the two spectra. The change induced in the spectrum by the presence of damage is illustrated in Figure 5a for severe damage, and in Figure 5b for mild damage. In these two figures, the 10–40 kHz band was presented, because it has clearly separated peaks, and hence is easier to examine visually. Figure 5a indicates that the presence of the crack in the close proximity of the sensor (*severe damage*) drastically modifies the pointwise frequency response function, and hence the real part of the E/M impedance spectrum. Resonant frequency shifts and the appearance of new resonances are noticed. In contrast, the presence of the crack in the far field (*mild damage*) only marginally modifies the frequency spectrum (Figure 5b). The same trends were observed in the other frequency bands, though the modal density was higher. Several overall-statistics damage metrics were tried: root mean square deviation (RMSD); mean absolute percentage deviation (MAPD); covariance change (CC); and correlation coefficient deviation $(1 - R^2)$. Figure 5c presents the plot of the cube of the correlation coefficient deviation, $(1 - R^2)^3$, damage metric calculated for the 300–450 kHz band. Among the overall-statistics damage metrics tested during our experiment, the $(1 - R^2)^3$ damage metric seemed to display the best performance: it monotonically decreases as the crack moves away from the sensor, and the decrease is almost linear. We concluded that:

1. The crack presence dramatically modifies the pointwise frequency response function, and hence the real part of the E/M impedance spectrum
2. This modification decreases as the distance between the sensor and the crack increases
3. A sensing circle of 80–100 mm diameter could be preliminarily assigned to this method, for the chosen specimens and crack configuration

However, the generalization of these results to other situations must be done with proper con-

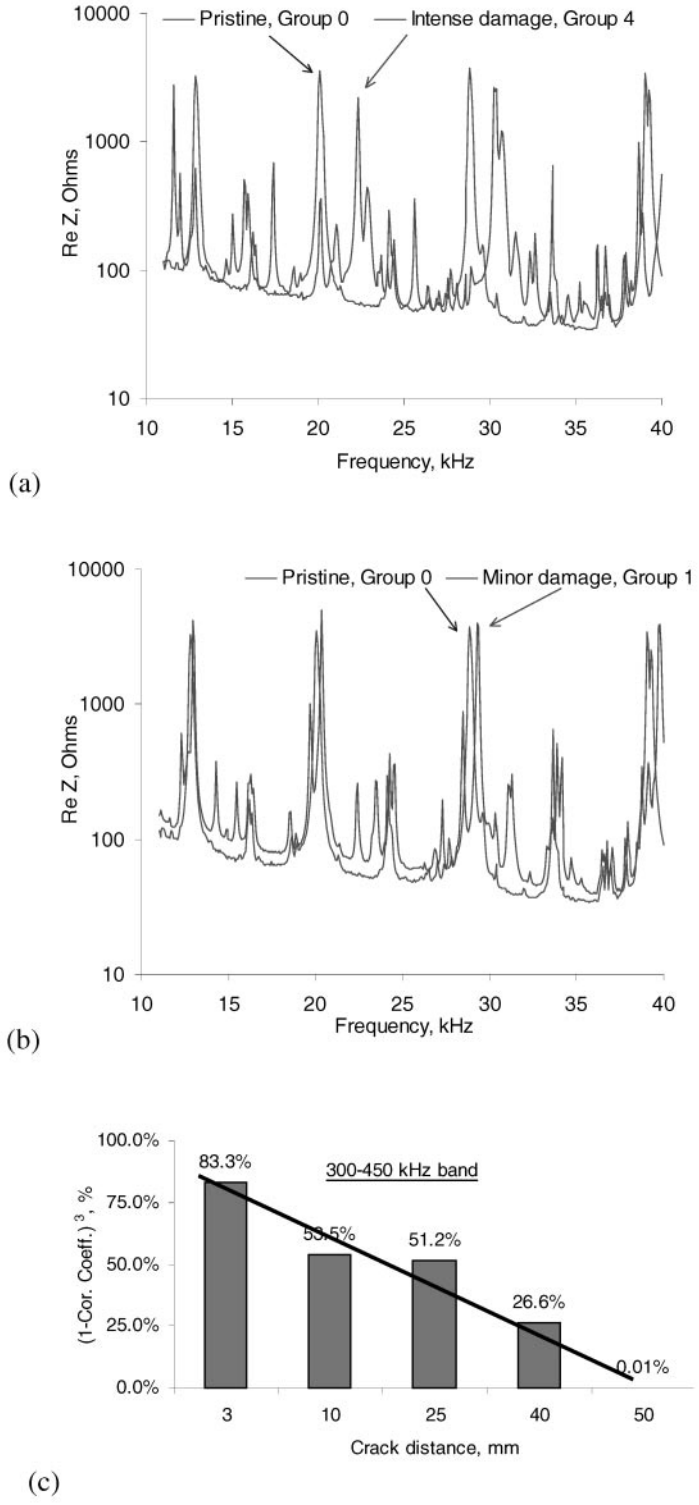

Figure 5 E/M impedance results: (a) superposed groups 0 and 4 spectra (10–40 kHz band); (b) superposed groups 0 and 1 spectra (10–40 kHz band); (c) damage metric variation with the distance between the crack and the sensor (300–450 kHz band).

sideration of the structural type, boundary conditions, and resonant frequencies range. In order to obtain consistent results, the proper frequency band (usually in high kHz) and the appropriate damage metric must be selected. For specific applications, systematic pre-tests investigations are needed to assess the frequency band to be used for data collection and the damage metric most appropriate for processing the frequency spectra.

5.2 E/M Impedance Damage Detection in Aging Aircraft Panels

Piezoelectric-wafer active sensors (PWAS) were applied to the realistic aging-aircraft panels to detect the change of E/M impedance spectrum induced by the proximity of a simulated crack. Figure 6 shows sensor installations: the sensors are placed along a line perpendicular to a 10-mm crack originating at a rivet hole. The sensors are 7-mm square and are spaced at 7-mm pitch. E/M impedance readings were taken for each sensor in the 200–2600 kHz range. Figure 6 also shows the frequency spectrum of the E/M impedance real part recorded during these experiments. The spectrum reflects clearly defined resonances that are indicative of the coupled dynamics between the sensors and the frequency-dependent point-wise structural stiffness as seen at each sensor location. The spectrum presented in Figure 6 shows high consistency. The dominant resonance peaks are consistently in the same frequency range, and the variations from sensor to sensor are consistent with the variations recorded during simple-plate calibration experiments.

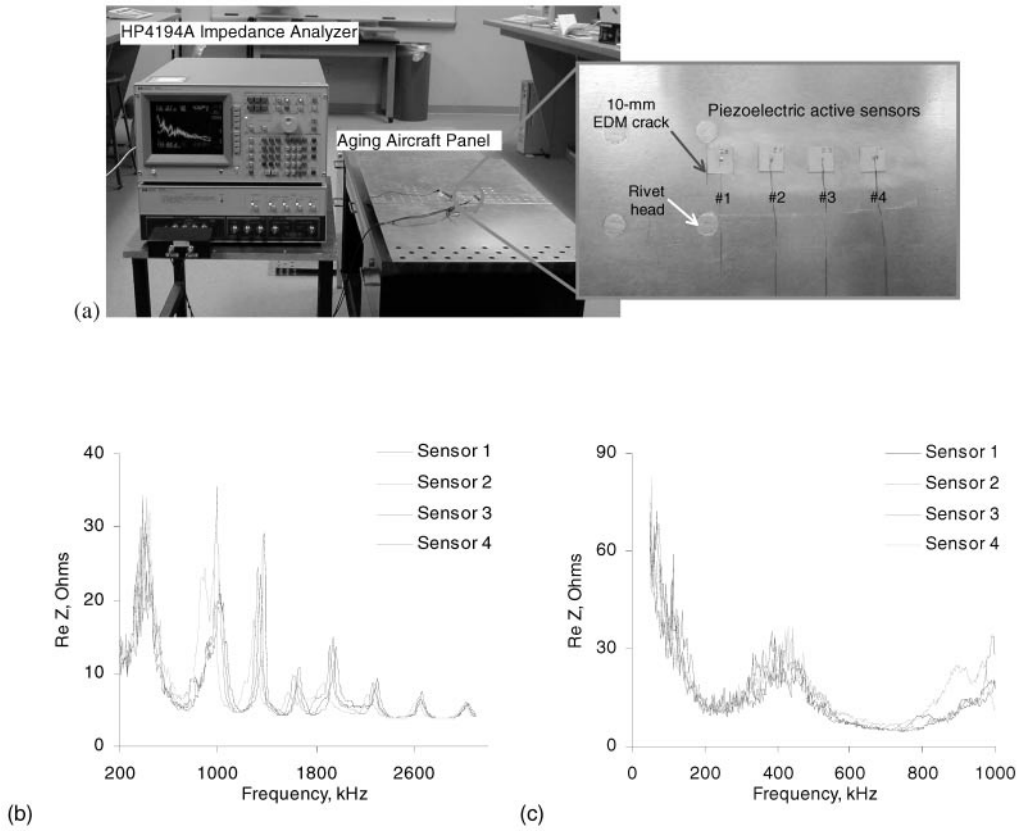

Figure 6 Detection of crack damage in aging aircraft panels using PWAS and the E/M impedance method: (a) Four PWAS placed at increasing distance from a 10-mm simulated crack (hairline EDM slit); (b) Re Z spectrum in the wide frequency band, 200–2600 kHz; (c) Re Z spectrum in the narrow frequency band, 50–1000 kHz.

Figure 6(b) shows the wide-band E/M impedance spectra for the four sensors (200–2600 kHz). It can be noted that the spectrum of sensor #1 (closest to the crack) has lower frequency peaks, which could be correlated to the presence of structural damage. However, this argument is not entirely self-evident since the spectra in Figure 6(a) also show other sensor-to-sensor differences that are not necessarily related to the crack presence. To better understand damage-detection aspects, further investigations were performed in a narrower frequency band, 50–1000 kHz (Figure 6(c)). In this band, we can identify the changes due to the crack presence as features in the sensor #1 spectrum that do not appear in the other sensors. For example, sensor #1 presents an additional frequency peak at 114 kHz that is not present in the other sensors. It also shows a downward shift of the 400 kHz main peak. These features are indicative of a correlation between the spectrum of sensor #1 and the fact that sensor #1 is placed closest to the crack. However, at this stage of the investigation, these correlations are not self evident, nor are they supported by theoretical analysis and predictive modeling of the structure under consideration. Further investigations are required to fully understand the correlation between the spectral features of the E/M impedance response and the presence of structural damage in the sensor vicinity.

5.3 E/M Impedance Damage-Detection Strategy

To understand the E/M impedance damage-detection strategy, consider an array of four PWAS. Incipient damage changes taking place in the structure are reflected in the drive-point structural impedance as seen by each sensor. Each PWAS has its own sensing area. This sensing area is characterized by a sensing radius and the corresponding sensing circle. Inside the sensing area, the sensor detection capability increases, as the sensor gets closer to the damage. A damage placed in the near field of the sensor is expected to create a larger disturbance in the sensor response than a damage placed in the far field. Effective area coverage is ensured when the sensing circles of several sensors overlap. The size of the sensing circle depends on the impedance of the sensor and the host structure, the material thickness, sensor size, excitation level, and material attenuation. The interrogation of the adjacent structure is performed using the active (real) part of the E/M impedance ($\mathrm{Re}\, Z$).

6 Wave-Propagation Damage-Detection Experiments

6.1 Wave Propagation Experiments on Simple-Geometry Specimens

Simple-geometry specimens were tested to understand the Lamb-wave detection methodology and to validate its assumptions (Figure 7). The specimens were constructed from 1.6 mm thick aircraft-grade 2024-T3 aluminum-alloy sheet. Two geometries were considered: (a) a narrow strip beam, 914 mm × 14 mm × 1.6 mm; and (b) a rectangular plate 914 mm × 504 mm × 1.6 mm. The specimens were instrumented with arrays of 7 mm square, 0.2 mm thick PWAS at five locations on the beam, and 11 locations on the plate as shown in Figure 7(a) and (b), respectively. The sensors coordinates are given in Table 2.

The experimental setup consisted of a HP 33120A signal generator, a Tektronix TDS 210 digital oscilloscope, and a laptop computer connected to the instruments through the GPIB interface (Figure 7(a)). The HP 33120A signal generator was used to generate Hanning-windowed tone bursts of 3 to 5 counts. The digital oscilloscope connected to the laptop was used for data collection. The 10 V peak-to-peak (pp) tone burst signal from the signal generator was applied directly to one of the PWAS. This PWAS, which acts as transmitter, generates elastic waves which travel through the specimen and are received by the other PWAS, which act as receivers. The transmitter can also act as receiver and sense the reflected elastic waves that come back to it (pulse-echo method). The beam experiments helped us understand the method. However, they are not very relevant for damage detection in realistic 2-D structures. The plate experiments were found more productive and relevant to 2-D structures. These experiments are discussed next.

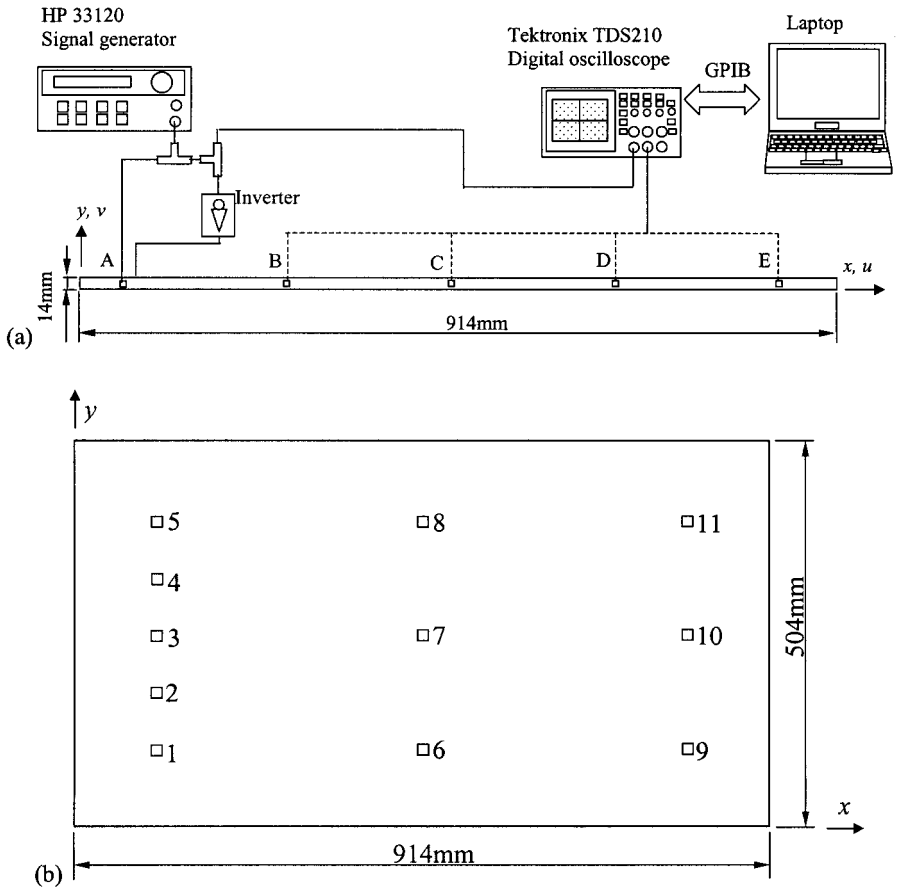

Figure 7 Simple geometry specimens: (a) narrow strip beam specimen of 1.6 mm thick 2024 aluminum alloy, 14 mm wide and 914 mm long. Shown are the five pairs of piezoelectric wafer active sensors (A through E); (b) rectangular plate specimen of 1.6mm thick, 2024 Aluminum alloy, 504 mm wide and 914 mm long.

Table 2 Locations of sensors on the thin rectangular plate specimen.

Sensor #	*1*	*2*	*3*	*4*	*5*	*6*	*7*	*8*	*9*	*10*	*11*
x (mm)	100	100	100	100	100	450	450	450	800	800	800
y (mm)	100	175	250	325	400	100	250	400	100	250	400

6.1.1 Frequency Tuning Effects The effect of excitation frequency on the wave amplitude of various Lamb-wave modes was investigated. It was found that, at low frequencies (e.g., 10 kHz) the excitation of the flexural waves (Lamb-wave A_0 mode) was much stronger than that of the axial waves (Lamb-wave S_0 mode). However, as frequency increases beyond 150 kHz, the excitation of flexural waves decreases, while that of the axial waves increases. A "sweet spot" for the axial-wave excitation was found in the 300–400 kHz range, as shown in Figure 8. At 300 kHz, the first wave pack and the axial pack peak together. The second wave pack peaks at 350 kHz.

6.1.2 Group Velocity Dispersion Curves The Lamb-wave group-velocity dispersion curves (Viktorov, 1967) were experimentally reproduced in the 10–600 kHz frequency band using the time-of-flight path-length correlation method. The raw

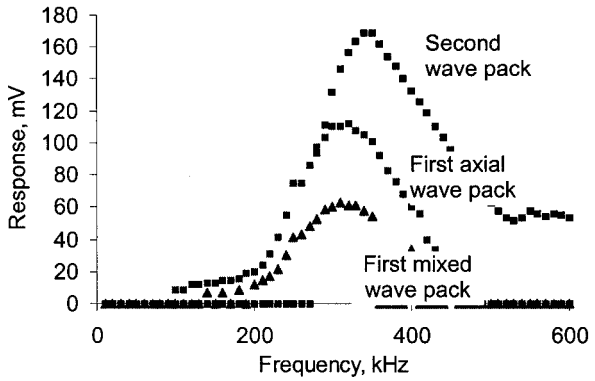

Figure 8 Frequency tuning studies identified a maximum wave response around 300 kHz.

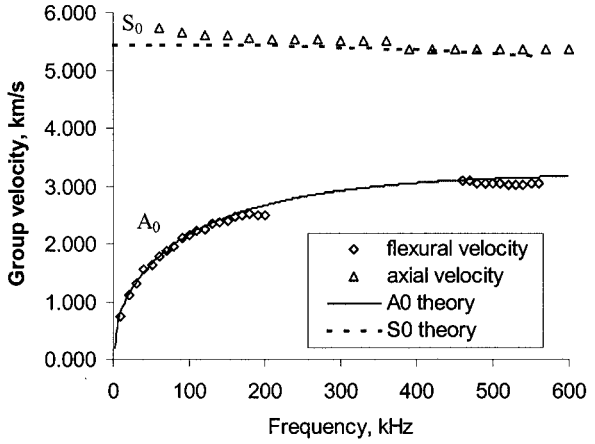

Figure 9 Group velocity dispersion curves for Lamb-wave A_0 and S_0 modes.

signals were processed using a narrow-band signal correlation algorithm followed by an envelope detection method. As a result, the exact TOF for each wave pack could be precisely identified. Figure 9 shows a plot of the group velocity vs. frequency resulting from our experimental measurements for the flexural and axial waves. Superimposed on the same chart are the A_0 and S_0 group velocities curves predicted by Lamb-wave theory (Viktorov, 1967; Giurgiutiu et al., 2001). The concordance between the theoretical A_0 group velocity and the measured A_0 group velocity is remarkably good. The A_0 data for the interval 200–450 kHz was not measured because, in this interval, the flexural wave could not be excited due to the axial wave's dominance (c.f., Figure 8). The S_0 data also shows remarkably good concordance with the theoretical predictions, except at low frequencies ($f < 100$ kHz) where the excitation of axial waves is more difficult due to the flexural wave's dominance. Overall, the data presented in Figure 9 indicates that the theoretical Lamb-wave group velocities predicted by the theory could be successfully reproduced experimentally.

One of the methods used in determining the group velocity is illustrated in Figure 10. Figure 10a shows the signals received at the PWAS #1 through #10 when PWAS #11 was excited with a 300 kHz Hanning-window smoothed tone-burst signal. The cleanness and consistency of the wave patterns are remarkable. In each signal, one notices a number of wave packs. The first of these packs corresponds to the wave received directly from the transmitter, PWAS #11. The subsequent wave packs correspond to waves reflected from the boundaries. The time of flight (TOF) of each wave pack seems to be consistent with the path length.

To verify TOF consistency and perform group velocity estimation, we determined TOF of the first-wave packs in each of the Figure 10(a) signals and calculated the corresponding wave path length (Table 3). When the path length was plotted against TOF (Figure 10b), a perfect straight line (99.99% R^2 correlation) was obtained. The slope of this line gives the experimental group velocity, $c_g = 5.446$ km/s. For the 1.6-mm aluminum alloy used in this experiment, the theoretical S_0-mode group velocity at 300 kHz is $c_{S0} = 5.440$ km/s. The speed-detection accuracy is remarkable (0.1%). Based on these group velocity determinations, we conclude that the first-wave packs observed in our experiments represent S_0 Lamb waves traveling in the thin-plate specimen.

6.1.3 Pulse-Echo Analysis During the plate experiments, pulse-echo analysis was also performed (Figure 11). The transmitter PWAS (#11) was used in a dual role: (a) to generate elastic waves ("initial bang"); and (b) to capture the echo signals of the waves reflected by the plate boundaries as they are coming back to the transmitter. Figure 11a shows the signal of PWAS

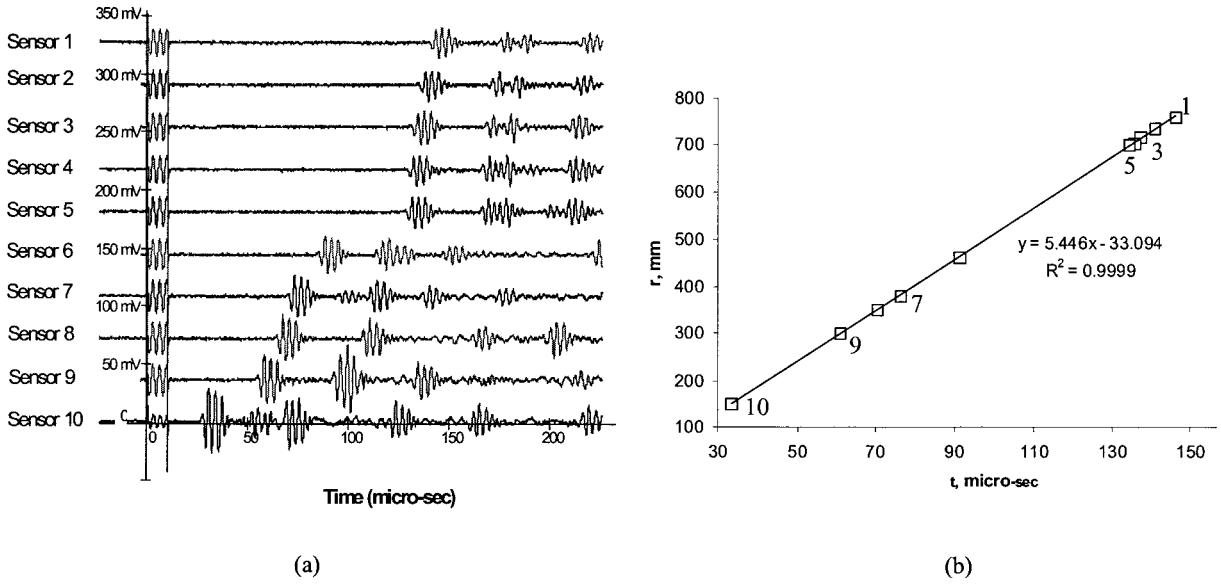

Figure 10 Signals observed during the rectangular plate experiments: (a) raw reception signals received at active sensors 1 through 10 when sensor 11 was excited with a 300 kHz smoothed tone burst; (b) time–distance correlation yields the wave group velocity with remarkable accuracy.

Table 3 Elastic wave reception data on the thin rectangular plate specimen.

Sensor #	x (mm)	y (mm)	r (mm)	TOF (μs)
1	70	0	70.0	221
2	84	0	84.0	263
3	98	0	98.0	302
4	112	0	112.0	357
5	200	0	200.0	537
6	200	96	221.8	602

#11, displaying the initial bang and a number of reflection wave packs. Figure 11b shows how the wave generated by the initial bang undergoes multiple reflections at the plate edges. These reflections and the corresponding path are identified by labels R_1 through R_8. The values of the true path length for these reflections are given in Table 4. It should be noted that the path lengths for reflections R_1 and R_2 have very close values. Hence, the echoes for these two reflections virtually superimpose on the pulse-echo signal (Figure 11a). It is also important to notice that the reflection R_4 has two possible paths, R_{4a} and R_{4b}. Both paths have the same length. Hence, the echoes corresponding to these two reflection paths arrive simultaneously and form a single-echo signal in Figure 11a. This explains why the reflection pack R_4 seems to have approximately double the intensity of the adjacent reflection packs. Figure 11c shows the TOF of the echo wave packages plotted against their path lengths. The straight line fit has a very good correlation ($R^2 = 99.99\%$). The corresponding group velocity value is 5.389 km/s, i.e., within 1% of the theoretical group velocity value of 5.440 km/s.

6.2 Wave Propagation Damage Detection in Aging Aircraft Panels

Wave propagation experiments were conducted on the realistic aircraft panel specimens with a number of PWAS affixed at various locations. The experimental apparatus was similar to that used for the wave propagation calibration experiments on simple geometry specimens (Figure 7). Several experiments were performed to verify the wave propagation properties, and to identify the reflections due to the construction features of the panels (rivets, splice joints, etc.) For illustration, Figures 12 and 13 present a crack detection

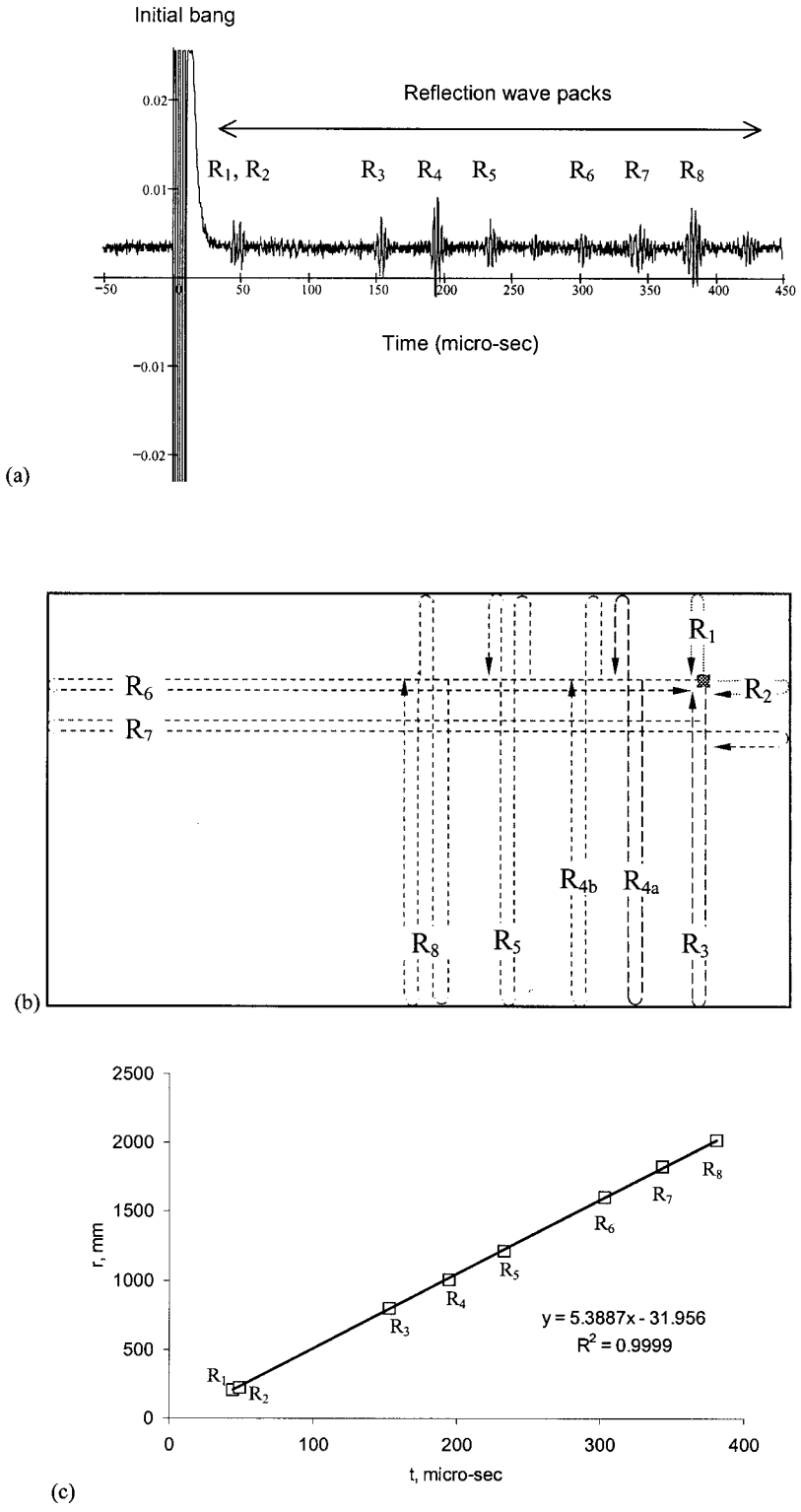

Figure 11 Pulse-echo method applied to active sensor #11: (a) the excitation signal and the echo signals on active sensor 11; (b) schematic of the wave paths for each wave pack; (c) correlation between path length and time of flight.

Table 4 Analysis of pulse-echo signals of sensor #11 on rectangular plate specimen.

Wave pack label	R_1	R_2	R_3	R_4	R_5	R_6	R_7	R_8
Time of flight (μs)	43.8	48.8	152.8	194.4	233.2	302.8	343.2	380.8
Path length (mm)	104	114	400	504	608	800	914	1008

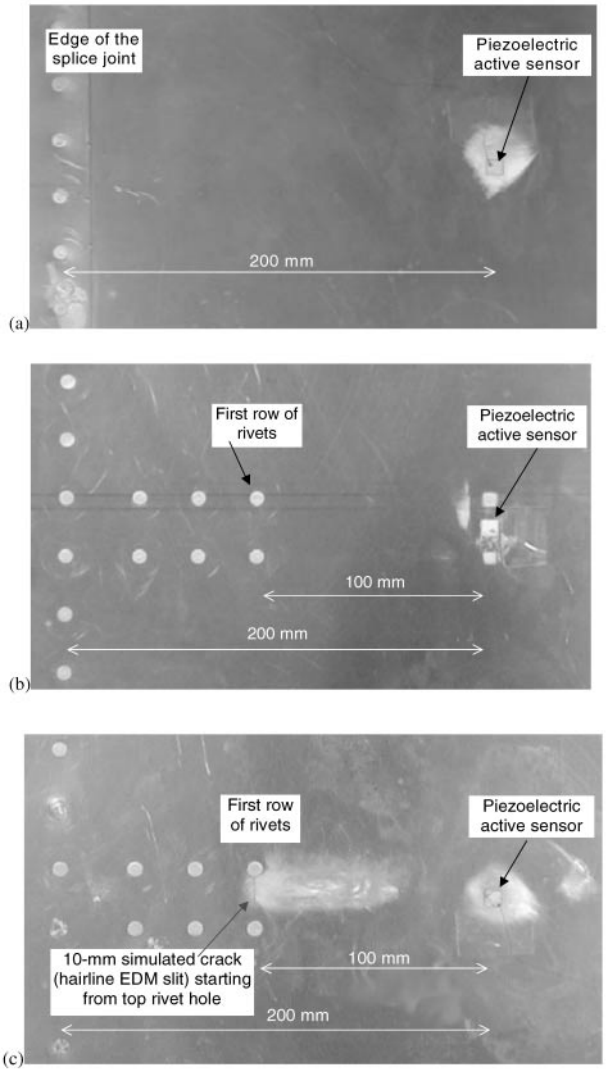

Figure 12 Crack detection experiment on aging aircraft panel: (a) pristine panel featuring an active sensor placed in a rivet-free region; (b) pristine panel featuring an active sensor placed at 100 mm from a row of rivets; (c) damaged panel featuring a 10 mm simulated crack (hairline EDM slit) starting from the top rivet.

example. Figure 12 shows three photographs of PWAS installation on increasingly more complex structural regions. Figure 12a shows the situation with the lowest complexity, in which only the vertical row of rivets is present in the far left. Figure 12b shows the vertical row of rivets in the far left and, in addition, a horizontal double row of rivets stretching over 100 mm distance. Figure 12c shows, in addition to everything shown in Figure 12b and, in addition, a simulated crack (10-mm EDM hairline slit) starting from the first rivet in the horizontal top row. This photo represents the damaged specimen. In all three regions, a PWAS was placed in the same relative location, i.e., at 200 mm to the right of the vertical row of rivets, which is at 100 mm from the start of the horizontal row of rivets. Consistent with the pulse-echo methods, the PWAS were used for both excitation and reception.

Figure 13 shows the analysis of the signals recorded during this experiment. Figure 13a shows the signal recorded in the region of Figure 12a. The signal shows the initial bang (centered at around 5.3 μs) and multiple reflections from the panel edges. The echoes start to arrive at approximately 60 μs. Figure 13b shows the signal recorded in the region shown in Figure 12b. In addition to the multiple echoes from the panel edges, this signal also features the echo from the rivets at the beginning of the horizontal double row. The echo from the rivets arrives at approximately 42 μs, indicating an approximate TOF = 37 μs. This TOF is consistent with a 5.4 km/s travel from the PWAS to the first line of rivets placed at 100 mm (200-mm total distance). Figure 13c shows the signal recorded on the damaged panel. It shows features similar to those of Figure 13c, but somehow stronger at the 42 μs position. These features correspond to the reflections from panel edges, the reflections from the rivets, and the reflection from the crack. The problem is especially difficult because the crack and the first row of rivets are at the same distance (100 mm) and hence their echoes superpose. However, by subtracting the signal of Figure 13b from that of Figure 13c, the effect

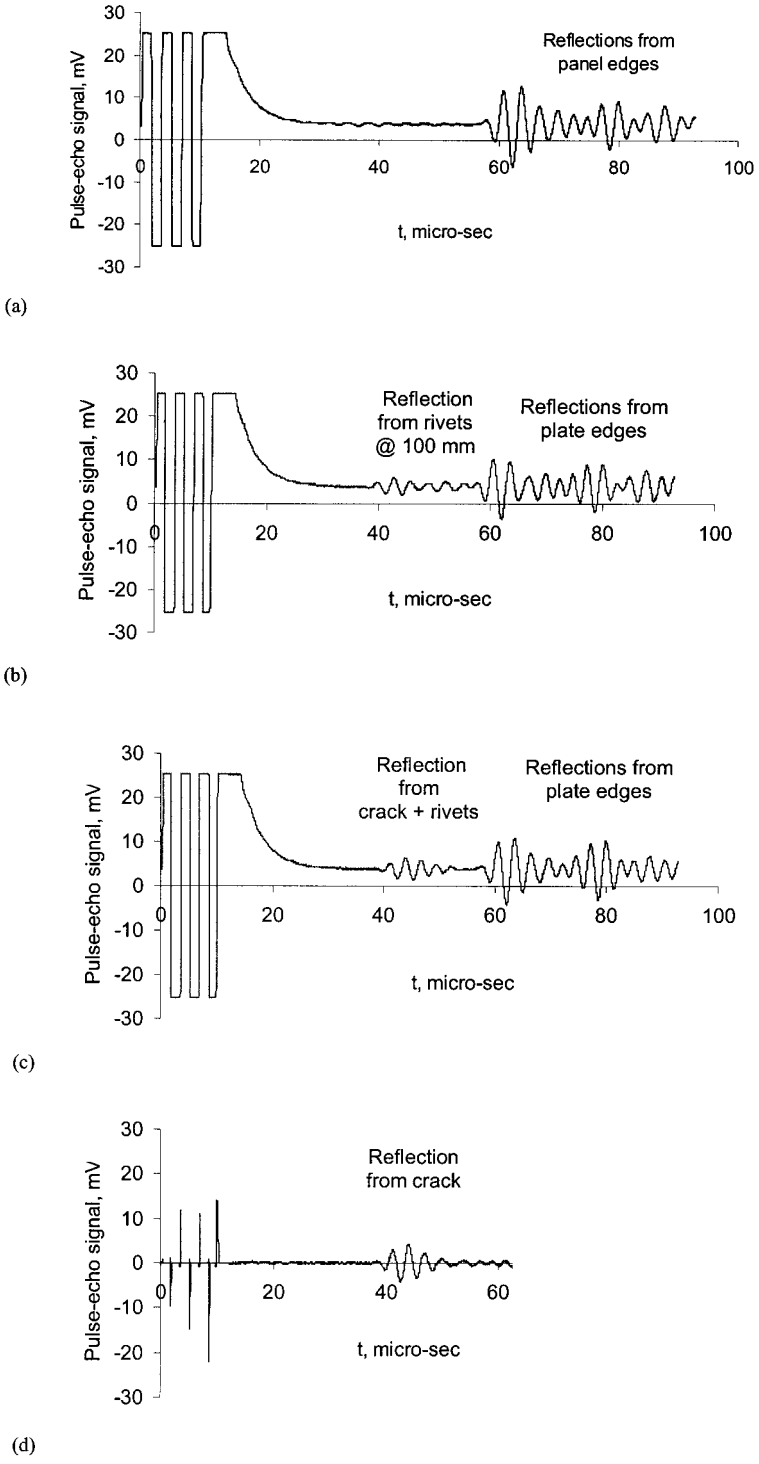

Figure 13 Analysis of the pulse-echo signals for crack detection: (a) signal showing only reflections from the panel edges; (b) signal recorded in the pristine panel featuring the reflection from the rivets and from the panel edges; (c) signal recorded on the cracked panel featuring, in addition, the reflections due to the presence of the crack; (d) signal difference revealing the strong reflection from the crack.

of the presence of the crack could be readily identified. The result of this subtraction is shown in Figure 13d, which features a strong wave pack centered on 42 μs, labeled "reflection from the crack". The cleanness of the crack-detection feature and the quietness of the signal ahead of the crack-detection feature are remarkable. Thus, we conclude that this method permits a clean and unambiguous detection of structural cracks.

6.3 Wave Propagation Damage Detection Strategy

To understand the wave-propagation damage-detection strategy, consider an array of four active sensors. Since PWAS can act as both transmitters and receivers, our strategy assumes that PWAS acts as a transmitter (#1) while the others act as receivers (#2, #3, and #4). PWAS #1 generates omnidirectional elastic waves. These propagate through the structure and are sensed at PWAS #2, #3, and #4. The properties of these waves are affected by the presence of damage, and can be interpreted to yield damage location and amplitude. To maximize the amount of data and mitigate the experimental error, a round-robin process is applied, whereby PWAS #2, #3, and #4 take, in turn, the function of wave generators, with the rest of the PWAS being wave sensors. This method can be applied to detect two types of damage: cracks and corrosion.

7 Implementation in Structural Health Monitoring Systems

We have seen that our health monitoring approach simultaneously uses two major strategies for structural-interrogation and damage detection:

1. *Local-area sensing with the E/M impedance method*, whereby each PWAS is excited independently. The PWAS E/M impedance is measured in a high frequency band (100–1500 kHz, depending on features size). The real part of the E/M impedance reflects the state of structural health in the local area inside the sensing of the PWAS. The integrity of the sensor itself is separately verified by the E/M impedance imaginary part.
2. *Wide-area sensing with wave propagation techniques* whereby the individual elements of a PWAS array are excited in a round-robin fashion and the elastic wave transmission through the structure is monitored. General acousto-ultrasonics methodology adapted to the embedded active-sensors architecture, and excitation by tone burst is proposed. The frequency band is selected consistent with the size of the feature (defect or damage) to be identified.

Note that the application of the proposed strategies to existing aging aircraft structures presumes the comparison between the current structure and a "pristine" structure. Such "pristine" structures could be defined as either a new structure (if available) or a structure that has been declared safe by the periodic NDI evaluation performed during the aircraft D-checks.

The small size of the PWAS also offers the possibility of multifunctional structural panels with integrated active-sensors and electronics (Noor et al., 1997). Such integrated structures could accommodate automated health monitoring systems that assess the structure on a green–yellow–red scale, locate the damaged area, and tele-transmit "structural health" bulletins to a central monitoring station for appropriate action. A stand-alone sensory array system containing local area network, data logging, data evaluation, tele-transmission, and historical data storage and processing is envisioned. The development of this concept is essential for the commercial implementation of the proposed methodology. For deployment on existing aging structures, the health monitoring system must be self contained and autonomous. To achieve this, the active-sensors array will be connected with a local set of embedded electronics properly packaged to fit into restricted space-envelopes. After local data is read, interpreted and evaluated, the diagnostic is sent to the transmitter and uplinked into a data logger that monitors a large number of sites and critical structures. In this way, only the

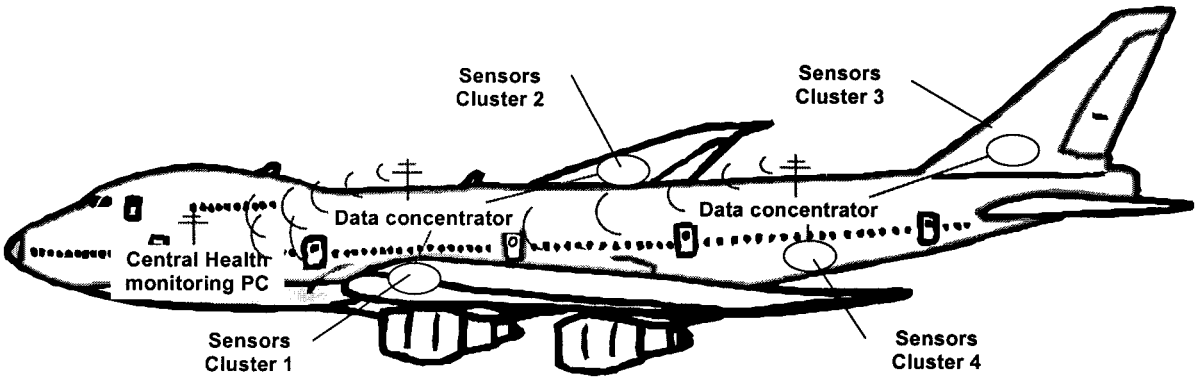

Figure 14 General concept of a sensor-array structural integrity monitoring system suggested installation on an aging aircraft.

essential health-diagnostic data (condition *green, yellow*, or *red*) is transmitted to the structural-integrity data bank to be logged into the structural integrity reports of the critical structural systems. Such an autonomous health-monitoring system would be ideally suited for incipient damage detection, and would have wide use in aerospace, automotive, civil infrastructure, and other industrial applications. A schematic of the proposed installation of such a system on a typical aging-aircraft is presented in Figure 14.

8 Summary and Conclusions

The development of inexpensive non-intrusive active sensors that can be applied on existing aging aerospace structures for monitoring the onset and progress of structural damage (fatigue cracks and corrosion) was presented. The state of the art in active sensors structural health monitoring and damage detection was reviewed. Methods based on (a) elastic wave propagation and (b) Electro-Mechanical (E/M) impedance were cited and briefly discussed.

Experiments were performed with a twin objective: (a) to validate the method on simple-geometry specimens; and (b) to illustrate the practical applicability of the method on realistic structural specimens representative of aging aerospace structures with seeded damage. The instrumentation of the specimens with PWAS, and methods for ensuring sensor integrity was presented. A novel sensor-self-diagnostics method was developed and experimentally verified. It was shown that, for a disbonded sensor, the imaginary part of the E/M impedance displays a clear resonance pattern that was not present in the perfectly bonded sensor. This sensor self-diagnostic method, disclosed by Giurgiutiu et al. (2002), is essential for reliable in-field implementation of the active-sensor structural health monitoring concepts.

For near-field damage detection, the E/M impedance method was used. The E/M impedance experiments showed that the real part of the E/M impedance spectrum is clearly influenced by the presence of damage (simulated crack). This behavior was explained in terms of the direct correlation between the pointwise mechanical impedance of the structure at the sensor location and the real part of the E/M impedance measured at the sensor terminals. Systematic experiments performed on 100 mm diameter thin-gage circular discs showed a direct correlation between the distance between the sensor and the crack. An overall-statistics damage index based on $(1 - R^2)^3$, where R^2 is the correlation coefficient between the "pristine" and the "damaged" E/M impedance real-part spectra, was developed. These findings were further substantiated by experiments performed on realistic aging aircraft panel using an array of four sensors placed at increasing distances from a 10-mm simulated crack. In these experiments, the effect of the crack was noticed as a left shift in the natural frequencies

for the sensor closest to the crack, and the appearance of a new frequency peak at around 114 kHz. However, additional efforts on advanced signal processing, identification of spectrum features, that are sensitive to the crack presence, and adequate modeling and simulation are still required to bring this method to full fruition.

For far-field damage detection, the use of PWAS for elastic wave transmission/reception was studied. Simple-geometry specimens were used to clarify the Lamb-waves generation mechanism, verify the group-velocity dispersion curves, and illustrate the pulse-echo method using the natural reflections from the specimen boundaries. Realistic aging-aircraft specimens were used to demonstrate how the method could be applied in practice. A 10-mm crack emanating from a rivet hole was detected with the pulse-echo method using a piezoelectric wafer active sensor placed at 100 mm from the damage location. The active sensor acted simultaneously as transmitter and receiver. Elastic waves in the 300 kHz band were used.

This study has shown that the E/M impedance method and the wave propagation approach are complementary techniques that should be simultaneously used for damage detection. Since the former method works in the near field, while the latter acts in the far field, their simultaneous utilization will ensure the complete coverage of the monitored structure. Concepts for a structural health monitoring system that could be implemented on an aging aircraft structure were presented. Damage detection strategies (E/M impedance for local area detection and wave propagation for wide area interrogation) were discussed. It was noted that, in the damage detection process, the signal processing methods and damage-metric algorithms have to be tuned to the specific structural interrogation techniques being used. In the high-frequency E/M impedance approach, pattern recognition methods should be used to compare the impedance signatures and to identify change in these signatures that are indicative of damage presence and progression. In the wave propagation approach, the pulse-echo and acousto-ultrasonic methods identifying the reflections generated from the damage site, and changes in wave phase and velocity, can be used. Both approaches would benefit from the use of artificial intelligence neural networks algorithm that can extract damage features based on a learning process. These research directions are currently being pursued and will be reported in future publications.

Acknowledgments

The financial support of Department of Energy through the Sandia National Laboratories, contract doc. # BF 0133 is thankfully acknowledged. Sandia National Laboratories is a multiprogram laboratory operated by Sandia Corporation, a Lockheed Martin Company, for the United States Department of Energy under contract DE-AC04-94AL85000.

References

ANSI/IEEE Std. 176 (1987). *IEEE Standard on piezoelectricity*, The Institute of Electrical and Electronics Engineers, Inc.

Ayres, T., Chaudhry, Z. and Rogers, C. (1996). Localized health monitoring of civil infrastructure via piezoelectric actuator/sensor patches. *Proceedings, SPIE's 1996 Symposium on Smart Structures and Integrated Systems, SPIE*, Vol. 2719 (pp. 123–131).

Bartkowicz, T.J., Kim, H.M., Zimmerman, D.C. and Weaver-Smith, S. (1996). Autonomous structural health monitoring system: a demonstration. *Proceedings of the 37th AIAA/ASME/ASCE/AHS/ASC Structures, Structural Dynamics, and Materials Conference*, Salt-Lake City, UT, April 15–17.

Blanas, P., Wenger, M.P., Rigas, E.J. and Das-Gupta, D.K. (1998). Active composite materials as sensing element for fiber reinforced smart composite structures. *Proceedings of the SPIE North American Conference on Smart Structures and Materials*, SPIE Vol. 3329, San-Diego, CA, March 1–5.

Blitz, Jack and Simpson, Geoff (1996). *Ultrasonic methods of non-destructive testing*, Chapman & Hall.

Boller, C., Biemans, C., Staszewski, W., Worden, K. and Tomlinson, G. (1999). Structural damage monitoring based on an actuator–sensor system. *Proceedings of SPIE Smart Structures and Integrated Systems Conference*, Newport CA, March 1–4.

Cawley, P. (1984). The impedance method for non-destructive inspection. *NDT International*, *17*(*2*), 59–65.

Chang, F.-K. (1995). Built-in damage diagnostics for composite structures. *Proceedings of the 10th International Conference on Composite Structures (ICCM-10)*, Vol. 5 (pp. 283–289). Whistler, B.C. August 14–18, Canada.

Chang, F.-K. (1998). Manufacturing and design of built-in diagnostics for composite structures. *52nd Meeting of the Society for Machinery Failure Prevention Technology*, Virginia Beach, VA, March 30–April 3.

Chang, F.K. (2001). Structural health monitoring: aerospace assessment. *Aero Mat, 12th ASM Annual Advanced Aerospace Materials and Processes Conference*, Long Beach CA, 12–13 June.

Chaudhry, Z., Sun, F.P. and Rogers, C.A. (1994). Health monitoring of space structures using impedance measurements. *Fifth International Conference on Adaptive Structures* (pp. 584–591). Sendai, Japan, 5–7 December.

Chaudhry, Z., Joseph, T., Sun, F. and Rogers, C. (1995). Local-area health monitoring of aircraft via piezoelectric actuator/sensor patches. *Proceedings, SPIE North American Conference on Smart Structures and Materials*, Vol. 2443 (pp. 268–276). San Diego, CA, 26 Feb.–3 March.

Deng, X., Wang, Q. and Giurgiutiu, V. (1999). Structural health monitoring using active sensors and wavelet transforms, Paper # 3667-35, SPIE's 6th Annual International Symposium on Smart Structures and Materials, Newport Beach, CA, 1–5 March.

Duke, J.C. Jr. (1988). *Acousto-ultrasonics – theory and applications*, Plenum Press.

Dupont, M., Osmont, R., Gouyon, R. and Balageas, D.L. (2000). Permanent monitoring of damage impacts by a piezoelectric sensor based integrated system, in *Structural Health Monitoring 2000* (pp. 561–570). Technomic.

Giurgiutiu, V. and Rogers, C.A. (1997). Electro-mechanical (E/M) impedance method for structural health monitoring an non-destructive evaluation. *Int. Workshop on Structural Health Monitoring* (pp. 433–444). Stanford University, CA, Sep. 18–20.

Giurgiutiu, V., Reynolds, A. and Rogers, C.A. (2000). Experimental investigation of E/M impedance health monitoring of spot-welded structural joints. Submitted for publication to the *Journal of Intelligent Material Systems and Structures*, *10*(*10*), 802–812.

Giurgiutiu, V. and Zagrai, A. (2000a). Characterization of piezoelectric wafer active sensors. *Journal of Intelligent Material Systems and Structures*, *11*(*12*), 959–976.

Giurgiutiu, V. and Zagrai, A. (2000b). Damage detection in simulated aging-aircraft panels using the electro-mechanical impedance technique. *Adaptive Structures and Materials Systems Symposium, ASME Winter Annual Meeting*, November 5–10, Orlando, FL.

Giurgiutiu, V., Bao, J. and Zhao, W. (2001). Piezoelectric-wafer active-sensor embedded ultrasonics in beams and plates. *Experimental Mechanics* (in press).

Giurgiutiu, V., Zagrai, A. and Bao, J. (2002). Piezoelectric wafer active sensors (PWAS), USC IPMO Invention Disclosure #00330/2002.

Ihn, J.-B. and Chang, F.-K. (2002). Built-in diagnostics for monitoring crack growth in aircraft structures. *Proceedings of the SPIE's 9th International Symposium on Smart Structures and Materials*, 17–21 March, San Diego, CA, paper #4702-04.

Jiang, Z., Kabeya, K. and Chonan, S. (1999). Longitudinal wave propagation measuring technique for structural health monitoring. *Proceedings of the SPIE Conference on Smart Structures and Integrated Systems*, Newport Beach, CA, March.

Krautkramer, Josef and Krautkramer, Herbert (1990). *Ultrasonic Testing of Materials*, Springer-Verlag.

Lange (1978). Characteristics of the impedance method of inspection and of impedance inspection transducers, *Sov. J. NDT*, pp. 958–966.

Liang, C., Sun, F.P. and Rogers, C.A. (1994). Coupled electro-mechanical analysis of adaptive material system-determination of the actuator power consumption and system energy transfer. *Journal of Intelligent Material Systems and Structures*, *5*, 12–20.

Lemistre, M., Gouyon, R., Kaczmarek, H. and Balageas, D. (1999). Damage localization in composite plates using wavelet transform processing on Lamb wave signals. *2nd International Workshop of Structural Health Monitoring* (pp. 861–870). Stanford University, September 8–10.

Lopes V. Jr., Park, G., Cudney, H. and Inman, D. (1999). Smart structures health monitoring using artificial neural network. *2nd International Workshop of Structural Health Monitoring* (pp. 976–985). Stanford University, September 8–10.

Moetakef, M., Joshi, S. and Lawrence, K. (1996). Elastic wave generation by piezoceramic patches. *AIAA Journal 34*(*10*), 2110–2117.

Monaco, E., Franco, F. and Lecce, L. (2001). Experimental and numerical activities on damage detection using magnetostrictive actuators and statistical analysis, *Journal of Intelligent Material Systems and Structures*, *11*(*7*), 567–578.

Noor, A.K., Venneri, S.L., Paul, D.B. and Chang, J.C.I. (1997). New structures for new aerospace systems. *Aerospace America*, November, pp. 26–31.

Osmont, D., Dupont, M., Gouyon, R., Lemistre, M. and Balangeas, D. (2000a). Damage and damaging impact monitoring by PZT sensors-based HUMS. *Proceedings*

of the SPIE Smart Structures and Materials 2000: Sensory Phenomena and Measurement Instrumentation for Smart Structures and Materials, SPIE Vol. 3986, (pp. 85–92).

Osmont, D., Devillers, D. and Taillade, F. (2000b). A piezoelectric based health monitoring system for sandwich plates submitted to damaging impacts. *European Congress on Computational Methods in Applied Sciences and Engineering ECCOMAS 2000*, Barcelona, 11–14 September.

Park, G., Cudney, H. and Inman, D.J. (2000a). Impedance-based health monitoring of civil structural components. *ASCE Journal of Infrastructure Systems*, *6(4)*, 153–160.

Park, G., Cudney, H. and Inman, D.J. (2000b). An integrated health monitoring technique using structural impedance sensors. *Journal of Intelligent Material Systems and Structures*, *11(6)*, 448–455.

Park, G., Cudney, H. and Inman, D.J. (2001). Feasibility of using impedance-based damage assessment for pipeline systems. *Earthquake Engineering and Structural Dynamics Journal*, *30(10)*, 1463–1474.

Quinn, P., Palacios, L., Carman, G. and Speyer, J. (1999). Health monitoring of structures using directional piezoelectrics. 1999 ASME Mechanics and Materials Conference, Blacksburg, VA, 27–30 June.

Staveley NDT Technologies (1998). Sonic Bondmaster™ product description, Kennewick, WA 99336, http://www.staveleyndt.com/prodset4.htm.

Sun, F.P., Liang, C. and Rogers, C.A. (1994). Experimental modal testing using piezoceramic patches as collocated sensors-actuators. *Proceeding of the 1994 SEM Spring Conference and Exhibits*, Baltimore, MI, June 6–8.

Sun, F.P., Chaudhry, Z., Rogers, C.A. and Majmundar, M. (1995). Automated real-time structure health monitoring via signature pattern recognition. *Proceedings, SPIE North American Conference on Smart Structures and Materials*, Vol. 2443 (pp. 236–247). San Diego, CA, 26 Feb.–3 March.

Tseng, K.K.-H., Bhalla, S. and Gupta, A. (2000). Performance of smart piezoceramic patches in health monitoring of a RC bridge. *Smart Materials and Structures*, *9*(*4*), 533–542.

Viktorov, I.A. (1967) *Rayleigh and Lamb waves*, New York: Plenum Press.

Wang, C.S. and Chang, F.-K. (2000). Built-in diagnostics for impact damage identification of composite structures. In: Fu-Kuo Chang (ed.), *Structural Health Monitoring*, 612–621.